Removal of phenolic compounds from aqueous solution using $MgCl_2$-impregnated activated carbons derived from olive husk: the effect of chemical structures

Imad Hamadneh, Rund A. Abu-Zurayk and Ammar H. Al-Dujaili

ABSTRACT

Activated carbon (BC) prepared from olive oil solid waste (olive husk) by slow pyrolysis was chemically activated using $MgCl_2$ (BC-$MgCl_2$). The BC and BC-$MgCl_2$ were used as adsorbents for removal of three phenolic compounds, namely, phenol (P), p-methoxyphenol (PMP) and p-nitrophenol (PNP), from aqueous solution. The uptake of these three phenolic compounds by the BC and BC-$MgCl_2$ was better expressed by the Langmuir and Dubinin–Radushkevich (D-R) isotherm models than by the Freundlich isotherm, and the kinetics of the adsorption process followed the pseudo-second order kinetic model. The maximum monolayer adsorption capacity of P, PMP and PNP were increased from 24.938, 45.455 and 61.728 on BC to 43.860, 98.039 and 121.951 mg/g on BC-$MgCl_2$ by factors of 1.76, 2.16 and 1.98, respectively. Therefore, the chemical activation of BC by $MgCl_2$ is indeed of importance for improving its adsorption performances. For both adsorbents, the adsorption phenomenon for different substituted phenols is a strong function of solubility, polarity, molecule structure, and size. At the tested temperatures (25, 35 and 45 °C), the negative values of ΔG° and positive values of ΔH° and ΔS° for the adsorption of P, PMP and PNP on BC and BC-$MgCl_2$ demonstrated that the adsorption was a spontaneous, endothermic and entropy-increasing process.

Key words | activated carbon, adsorption, chemical activation, magnesium chloride, olive waste

HIGHLIGHTS

- Activated carbon (BC) was prepared from olive husk biomass by slow pyrolysis at 630°C.
- BC was chemically activated with magnesium chloride to produce activated carbon.
- Phenol, p-methoxyphenol and p-nitrophenol biosorption was performed in a batch method.
- Biosorption was well described by the Langmuir and Dubinin–Radushkevich (D-R) isotherm models.
- Biosorption kinetics of phenols was found to follow the pseudo-second order model.

Imad Hamadneh
Department of Chemistry, Faculty of Science,
University of Jordan,
Amman 11942,
Jordan

Rund A. Abu-Zurayk
Ammar H. Al-Dujaili (corresponding author)
Hamdi Mango Center for Scientific Research,
University of Jordan,
Amman 11942,
Jordan
E-mail: *ah.aldujaili@gmail.com*

doi: 10.2166/wst.2020.297

GRAPHICAL ABSTRACT

INTRODUCTION

The olive oil industry has witnessed rapid expansion over the past two decades (International Olive Council 2015). Jordan is the eighth largest producer of olive oil in the world. Olive oil farming provides vital economic benefits to the country and small farmers. Nevertheless, fast growth combined with unplanned and poor environmental management practices by olive-press factories has led to serious consequences on the surrounding environment. Therefore, it is important to find a low-cost, low-technology method to use treated wastewater and leachate from the olive mill. The olive cake is a lignocellulosic material that can be processed to generate useful products such as activated carbon (El Hanandeeh 2013). Interest in activated carbon production as a method for soil carbon sequestration as well as a soil amender has been growing (Lehmann *et al.* 2011). Activated carbon has also been suggested as a potential low-cost alternative to activated carbon for the removal of contaminants from water and wastewater (Tan *et al.* 2015).

Activated carbon is a low-cost material that can be produced from many organic sources, including agricultural waste (Zhang *et al.* 2014). It has great capacity to adsorb organic and inorganic sewage contaminants (Mohan *et al.* 2014; Tan *et al.* 2015). Activated carbon characteristics, however, are extremely dependent on the circumstances of parent biomass and preparation (Cha *et al.* 2016).

Many researchers studied the capacity of activated carbon prepared from olive oil solid waste (also known as olive husk and olive cake) to remove organic contaminants form wastewater. Baccar *et al.* (2012) studied the capacity of activated carbon prepared from olive-waste cakes to remove pharmaceutical compounds – ibuprofen, ketoprofen, naproxen and diclofenac – from water at 25 °C. They concluded that the equilibrium data best fit with the Langmuir isotherm model and the adsorption capacities of the activated carbon for the four drugs was reduced with increasing of pH and temperature. The removal capacity for dodecylbenzenesulfonic acid–sodium salt detergent (DBSNa) and methylene blue dye (MB) of olive cake was investigated (Cimino *et al.* 2005). The results showed that acidic treatment changes the surface properties of olive cake but does not enhance its adsorption capacity. Compared to commercial activated carbons the olive cake activated carbon generally is equally able to uptake MB and DBSNa from solution. Recently, the role of olive cake activated carbon to remove acid blue 80 dye, methylene blue and basic yellow 28 (BY28) was investigated by Toumi *et al.* (2018a, 2018b) who reported that the experimental adsorption isotherms show the presence of two steps, depending on these compounds' concentration. They further claimed that the interactions between activated carbon and these dyes were identified by molecular simulations as hydrogen, Van der Waals and electrostatic bonds. Weidemann *et al.* (2018) used olive-press wastes activated carbon to remove 10 compounds of environmental concern (octhilinone, triclosan, trimethoprim, sulfamethoxasole, ciprofloxacin, diclofenac, paracetamol, diphenhydramine, fluconazole, and bisphenol A) from aqueous solution. They have found that the adsorption capacity tests revealed that removal efficiencies varied substantially among different materials.

The removal of phenols from aqueous solutions using activated carbon was investigated by several researchers (Hall *et al.* 2014; Sy & Yd 2016; Li *et al.* 2017). Activated carbon prepared at pyrolytic temperatures, 700 °C, from bamboo chips was used to remove polycyclic aromatic hydrocarbons, nitrobenzenes, phenols, and anilines from aqueous solution. The impacts on adsorption ability of

organic molecular dimensions and melting points are attributed respectively to the molecular sieving impact and the holding effectiveness of organic molecules in the pores of the activated carbon (Yang *et al.* 2016). Han *et al.* (2013) investigated the efficacy of halogenated phenols using activated carbon prepared from bio-solids, fallen leaves, rice straw, corn stalk and used coffee grounds over a pyrolytic temperature range between 250 and 550 °C. They explained that the removal efficiency was limited because of the high pH and low surface area of activated carbon as well as the deprotonation of phenols in the activated carbon system. Nevertheless, the adsorption capacity of phenol on activated carbon was directly related to the surface area and surface charge. Recently, Vunain *et al.* (2018) reported the feasibility of remediation of catechol- and resorcinol-contaminated water using low-cost sunflower seed hull activated carbon. They have found that at the same experimental conditions, more catechol was adsorbed than resorcinol, which may be due to the catechol's affinity towards water and the position of the hydroxyl group on the benzene ring.

A limited number of studies on the capacity of activated carbon prepared from olive husk for the removal of phenolic compounds have been reported (Cimino *et al.* 2005; Michailof *et al.* 2008; Abdel-Ghani *et al.* 2016). For example, Cimino *et al.* (2005) reported the potential of activated carbon prepared from olive husk for the removal of phenol from aqueous solution under various conditions. The results showed that the activation of activated carbon by HCl changes the surface properties of olive cake and enhances its sorption capacity. Olive husk was used by chemical activation with KOH to prepare activated carbon. This activated carbon has been used to adsorb a polyphenol combination. The function of porosity and surface groups in the adsorption forces and the characteristics of adsorbed substances was discussed (Cimino *et al.* 2005). Abdel-Ghani *et al.* (2016) evaluated the removal of *p*-nitrophenol by adsorption onto olive cake based activated carbon having a high Brunauer–Emmett–Teller (BET) surface area. The results of this study proved the efficiency of using olive cake based activated carbon as a novel adsorbent for the removal of nitrophenol from aqueous solution.

Given the results of our previous study (El Hanandeh *et al.* 2016) on the effect of pyrolysis temperature on the preparation of activated carbon from solid waste from Jordanian olive oil processing (OOSW), the optimum temperature of 630 °C was selected. This sample was activated with $MgCl_2$ in this work to study the effect of chemical activation. Thus, there are two main objectives of the present work. The first was to prepare activated carbon from OOSW by chemical activation with $MgCl_2$ to obtain an abundant agricultural by-product, green and environmentally friendly low-cost activated carbon. The second was to reveal the effect of substituents on the adsorption of phenol (P), *p*-methoxyphenol (PMP) and *p*-nitrophenol (PNP) on BC and BC-$MgCl_2$. Batch adsorption experiments were carried out under various operational conditions such as pH of phenols, ionic strength, contact time, adsorption temperature and adsorbent dosage.

EXPERIMENTAL

Materials

Reagent-grade hexahydrate $MgCl_2$, P, PMP and PNP were obtained from Sigma Aldrich (Buchs, Switzerland), with purity higher than 99%, and were used without further purification. Deionized water was used in the present study.

Instrumentation

Activated carbon preparation was conducted using a Protherm-PC 402 tube furnace model, Turkey. Sample weighing was performed using the analytical balance Precisa 410AM-FR. Using a EuroVector elemental analyzer, elemental analysis of coal, hydrogen and nitrogen was performed. The spectrum of Fourier transform infrared (FTIR) spectroscopy was registered using the Thermo Nicolet NEXUS 670 FTIR spectrophotometer. Using PANalytical's X'Pert PRO X-ray diffraction (XRD) system at 40 kV and 30 mA with a step of 0.02° over the range of 4–60°, the samples were examined using an X-ray powder diffractometer with Cu K range radiation ($\alpha = 1.5418$ Å). Using FEI Inspect F50 scanning electron microscopy (SEM), the sample shape and surface morphology were examined. The sampling was performed using the GFL 1083 shaker. Shaking was done using the thermostat-equipped GFL 1083 shaker. Using the UV-Vis Cary Varian spectrophotometer, phenol levels were determined.

Preparation of activated carbon

The activated carbon was prepared in the laboratory from olive husk obtained from a modern olive press in northern Jordan. Pyrolysis of olive husk was carried out at 630 °C pyrolysis temperature under oxygen-limited conditions for the duration of 1 h and labeled as BC. The prepared BC was stored in air-tight containers for further uses.

Activation

Activated carbon's chemical activation was carried out using $MgCl_2$. The impregnation ratio was calculated as the weight ratio of $MgCl_2$ to the weight of the biomass used. Eighty grams of $MgCl_2$ was dissolved in 250 mL of distilled water, and 20 g of biomass was then mixed with the $MgCl_2$ solution and stirred for 24 hours at about 80 °C to guarantee a full response with $MgCl_2$. Then the mixtures were filtered and for about 24 h the remaining solids were dried at 105 °C. Impregnated sample pyrolysis was performed at 630 °C for 1 h. The resulting solid was boiled at about 90 °C after pyrolysis with a solution of 100 mL of 1 M HCl for 30 min to drain the activating agent, filtered and rinsed several times with hot distilled water until the pH value was 6–7. The yield of activated carbon was calculated based on the weight of olive husk on a dry basis from the following equation:

$$\text{Percentage yield } (\%) = \frac{\text{weight of activated carbon}}{\text{weight of olive husk}} \times 100 \quad (1)$$

Ash and moisture content were determined by weight difference according to the following equations (Gaya *et al.* 2015):

$$\text{Moisture content } (\%) = \frac{W_1 - W_3}{W_2 - W_1} \times 100 \quad (2)$$

$$\text{Ash content } (\%) = \frac{W_2 - W_3}{W_2 - W_1} \times 100 \quad (3)$$

where W_1 is the weight of crucible, W_2 is the initial weight of crucible with sample and W_3 is the final weight of crucible with a sample. The percentage yield, moisture and ash content of activated carbon were expressed as the average of three experiments by ± standard deviation.

The pH of BC and BC-$MgCl_2$ was measured by a pH meter (HI9025) and the measurements were carried out in triplicate at 25 °C. The pH at point of zero charge (pH_{pzc}) of the BC and BC-$MgCl_2$ adsorbent was determined by solid addition method (Mall *et al.* 2006) by transferring 50 mL KNO_3 to a series of 100 mL conical flasks. This solution's original pH (pH_i) was adapted approximately from 2 to 10 with either 0.1 M HNO_3 or 0.1 M NaOH solutions. The solution's pH_i was correctly measured and 0.1 g of BC or BC-$MgCl_2$ was added to each flask. The flasks were permitted to balance with intermittent manual shaking for 24 hours. The supernatant liquid's final pH (pH_f) values were measured. The difference between pH_i and pH_f values was plotted against pH_i. The intersection of the resulting curve at the point where the pH difference = 0 is the pH_{pzc}.

The physicochemical parameters, volatile matter content (%), acid extractable content and fixed carbon (%), were determined according to the procedures given in our previous publication (El Hanandeh *et al.* 2016).

Preparation of P, PMP and PNP solution

Stock solution (500 mg /L) was prepared individually for P, PMP and PNP by dissolving the necessary amount in 0.01 M NaCl. The stock solutions were used to prepare solutions with distinct levels (10–100 mg/L); the dilution was achieved by using 0.01 M NaCl solution (to maintain the ionic strength constant for all the different concentrations). The solution's pH was adapted with solutions of 0.1 M HCl and NaOH.

Determination of specific surface area

The sample surface area of the pore structure of BC and BC-$MgCl_2$ was assessed using a Nova 2200e surface area and pore size analyzer (Quantachrome Corp., Boynton Beach, FL, USA) from nitrogen gas adsorption isotherms analysis at 77 K. Each sample was degassed at 105 °C for 8 hours. BET equations determined the particular surface area (SA_{BET}) and calculated the complete pore quantity from the near-saturation uptake (relative pressure (pressure of the adsorbate relative to its saturation pressure) = 0.99). The mesopore volume, mesopore surface area (SA_{meso}), and pore size distribution were calculated by the Barret, Joyner, and Halenda method.

Adsorption experiment

A batch experiment was carried out by shaking BC or BC-$MgCl_2$ with 50 mL aqueous solution of P, PNP and PMP in the presence of adsorbent dose of 0.20 g/50 mL, to determine the effects of various process parameters, different conditions of pH (from 2.0 to 11.0), contact time (5–240 min), ionic strength (0.01–0.20 M) and temperature (25, 35, 45 °C). Initial P, PMP and PNP concentrations (10–100 mg/L) were prepared by proper dilution from the stock 500 mg/L phenols standard. The pH of solution was adjusted until the equilibrium was achieved. Narrow-neck, dark-brown coloured bottles were used to prevent

photooxidation. At the end of the desired equilibrium period the contents of the bottles were filtered by a micro filter, and centrifuged for 5 min at 3,500 rpm using a Hermle centrifuge model Z200A (Germany). The equilibrium concentration of phenols was measured spectrophotometrically on a UV spectrophotometer at wavelengths 269, 288 and 285 nm for P, PMP and PNP, respectively. The reproducibility of the data varied in the range of ±1.5%. The adsorption capacity for P, PMP and PNP of BC and BC-$MgCl_2$ (q_e, mg/g) was calculated by Equation (4):

$$q_e = \frac{(C_i - C_e)V}{m} \tag{4}$$

The percentage removal values were calculated using Equation (5):

$$\%\text{Removal} = \frac{(C_i - C_e)}{C_i} \times 100 \tag{5}$$

where q_e is the amount of phenols in mg retained by 1 g of the adsorbent; C_i is the original concentration (mg/L); C_e is the balance concentration (mg/L) of the phenols in the m g of adsorbent.

Adsorption equilibrium and kinetics models

Three most popular isothermic adsorption models portraying the adsorption isotherms of P, PMP and PNP on BC and BC-$MgCl_2$ adsorbent, Langmuir, Freundlich and Dubinin–Radushkevich (D-R), were used.

Langmuir isotherm model (Langmuir 1918):

$$q_e = \frac{q_{max} K_L C_e}{1 + K_L C_e} \tag{6}$$

Freundlich isotherm model (Freundlich 1906):

$$q_e = K_F C_e^{1/n} \tag{7}$$

D-R isotherm model (Dubinin *et al.* 1947):

$$q_e = q_{max} \exp\left(-K_{DR}\left[RT \ln\left(1 + \frac{1}{C_e}\right)\right]^2\right) = q_{max} \exp\left(-K_{DR}\varepsilon^2\right) \tag{8}$$

where q_e is the quantity of P, PMP and PNP absorbed by the adsorbents (mg/g), q_{max} is the monolayer capacity of the adsorbent (mg/g), K_L is the Langmuir binding constant (L/mg), K_F is the Freundlich constant [$mg{\cdot}g^{-1}(L{\cdot}mg^{-1})1/n$] indicating the adsorption capacity, n is the empirical constant indicating the adsorption intensity, ε is the polanyi potential equivalent to $RT \ln(1 + 1/C_e)$, K_{DR} is related to the mean free adsorption energy per molecule of adsorbate, R are T are the gas constant (8.314 J/mol·K), and temperature (K), respectively. E_{DR} (kJ/mol) is the mean free adsorption energy per adsorbent molecule when transmitted from infinity to the solid surface in the solution, which offers chemical or physical adsorption data and can be determined by the following equation:

$$E_{DR} = (2K_{DR})^{-1/2} \tag{9}$$

The pseudo-first order and pseudo-second order kinetic models were used to explore the best fit of the experimental information extracted from the adsorption of P, PMP and PNP.

Lagergren pseudo-first order kinetic model (Lagergren 1898):

$$q_t = q_e(1 - e^{-k_1 t}) \tag{10}$$

Pseudo-second order model (Hubbe *et al.* 2019):

$$q_t = \frac{k_2 q_e^2 t}{1 + k_2 q_e t} \tag{11}$$

where q_t (mg/g) is the quantity of P, PMP and PNP adsorbed at any time, k_1 is the pseudo-first order constant (1/min) and k_2 is the pseudo-second order adsorption equilibrium constant (g/mg·min).

The nonlinear fitting technique was used to standardize equilibrium and kinetic models. Values of determination coefficient (R^2) and chi-squared (χ^2) were recommended (Tran *et al.* 2017a).

$$R^2 = 1 - \frac{\sum (q_{e,Exp.} - q_{e,Calcd.})^2}{\sum (q_{e,Exp.} - q_{e,mean})^2} = \frac{\sum (q_{e,Calcd.} - q_{e,mean})^2}{\sum (q_{e,Calcd.} - q_{e,mean})^2 + \sum (q_{e,Calcd.} - q_{e,Exp.})^2} \tag{12}$$

$$\chi^2 = \sum \frac{(q_{e,Exp.} - q_{e,Calcd.})^2}{q_{e,Calcd.}} \tag{13}$$

Furthermore, models were also assessed using an error function (Vaghetti *et al.* 2009) which measures the variations

in the quantity of P, PMP and PNP taken up by the adsorbent predicted by the models and the real q_e measured experimentally.

$$F_{error\%} = 100 \times \sqrt{\sum_{i}^{N} \left[\frac{q_{e,Exp.} - q_{e,Calcd.}}{q_{e,Exp.}}\right]^2 / (N - P)} \quad (14)$$

where $q_{e,Exp.}$ (mg/g) is the equilibrium quantity of phenols extracted from Equation (13), $q_{e,Calcd.}$ (mg/g) is the quantity of phenols extracted from the models and $q_{e,mean}$ (mg/g) is the mean of $q_{e,Exp.}$values; N is the number of experimental information points, P is the number of model parameters.

RESULTS AND DISCUSSION

Characterization of BC and BC-$MgCl_2$

The effects of impregnation on the physicochemical properties including activated carbon yield, moisture content, volatile matter content%, acid extractable sample, ash content, pH, pH_{pzc} and elemental analysis are listed in Table 1. The pH value of the BC decreased from 10.22 to 8.69, which is consistent with the depressed ash content (84.95–57.34%) as the result of impregnation. The pH_{pzc} of the activated carbons was found to be lowered from 9.71 to 6.92. The carbon content of BC-$MgCl_2$ substantially increased from 62.45 to 76.29 wt.% after the activation process. Hydrogen and oxygen contents showed the opposite change trend, as expected due to the release of volatiles during carbonization, which results in the elimination of non-carbon species and enrichment of carbon. These results are consistent with the findings of other research studies using $MgCl_2$ or $ZnCl_2$ as a chemical activated agent (Angin *et al.* 2013; Cardoso & Ataide 2015; Tazibet *et al.* 2018).

The effects of impregnation with $MgCl_2$ on the surface area and pore size analysis of the activated carbons were shown in Table 2. The results reveal that the SA_{BET} and SA_{meso} of the BC before impregnation were 53 and 14 m^2/g, while after impregnation they were raised to 267 and 109 m^2/g, respectively, which indicates that the surface area of the BC increased after impregnation. Total pore (V_{total}) and mesopore volumes (V_{meso}) and particle diameter (Dv) of BC-$MgCl_2$ also increased with the impregnation. The method of activation appears to be improving pore growth and creating fresh pores. Similar findings have been noted by Ucar *et al.* (2009) and Angın *et al.* (2013), where the rise in surface region and impregnated pore volumes indicates that porosity produced by $MgCl_2$ may be due to pore widening and mesopore formation left by magnesium chloride following acid and water washing.

The XRD for BC and BC-$MgCl_2$ are shown in Figure 1. The BC pattern displayed a very noisy, amorphous structure with some peaks appearing at $2\theta = 40.99$, 42.82, 43.61,

Table 1 | The physicochemical properties of the BC and BC-$MgCl_2$

Parameter	Average value	
	BC	BC-$MgCl_2$
Yield (%)	26.37	41.74
Moisture content (%)	5.19	9.86
Volatile matter content (%)	17.42	15.56
Acid extractable sample	16.41	8.98
Ash content (%)	84.95	57.34
pH	10.22	8.69
PH_{pzc}	9.71	6.92
Specific surface area (m^2/g)	24	89
Fixed carbon (%)	71.25	79.58
C (%)	62.45	76.29
H (%)	2.26	1.85
N (%)	4.07	2.48
O (%)[a]	31.22	19.38

[a]Calculated by difference.

Table 2 | Textural parameters of the BC and BC-$MgCl_2$

Biochar	SA_{BET} (m^2/g)	SA_{meso} (m^2/g)	V_{total} (cm^3/g)	V_{meso} (cm^3/g)	Pore diameter (nm)
BC	69.019	9.717	0.027	0.010	1.385
BC-$MgCl_2$	483.642	112.885	0.038	0.066	1.532

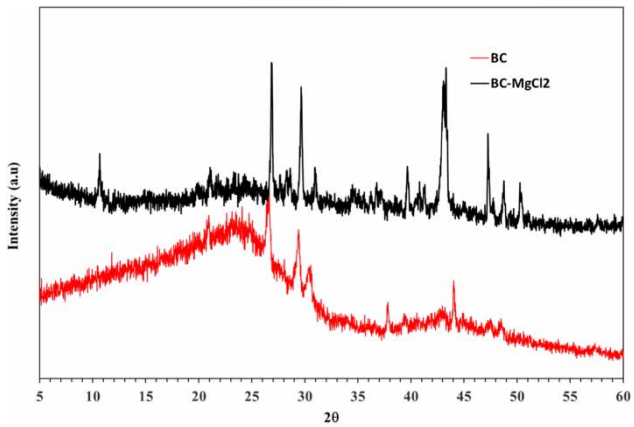

Figure 1 | XRD of BC and BC-$MgCl_2$.

47.51 and 57.38°. Extra peaks appeared at $2\theta = 14.61$, 35.10°, and 50.54°, which belong to $MgCl_2$ in BC-$MgCl_2$ where the peak resulted from enhancement to the crystallinity. The surface morphological structure of activated carbons before and after activation was examined using SEM. Figure 2 shows that BC has smooth surface without distinctive pores (Figure 2(a)). Activation of the BC produced an irregular and heterogeneous surface morphology with a well-developed porous structure in various sizes as shown in Figure 2(b). Thus, it seems that the cavities resulted from the evaporation of $MgCl_2$ residues and other impurities such as MgO during carbonization, leaving the space previously occupied by the $MgCl_2$ and MgO. Similar results have also been reported by other researchers (Yang & Lua 2006; Ucar *et al.* 2009).

It is well known that the surface functional groups would give insight into the adsorption capability of the produced activated carbon. The FTIR spectra obtained for BC and BC–$MgCl_2$ (Figure 3) were determined to be similar, which indicates that the same surface functional groups and structures are present in the BC and BC–$MgCl_2$ prepared at the same temperature. However, significant differences concerning the relative intensity of bands are observed between both spectra. The broad absorption

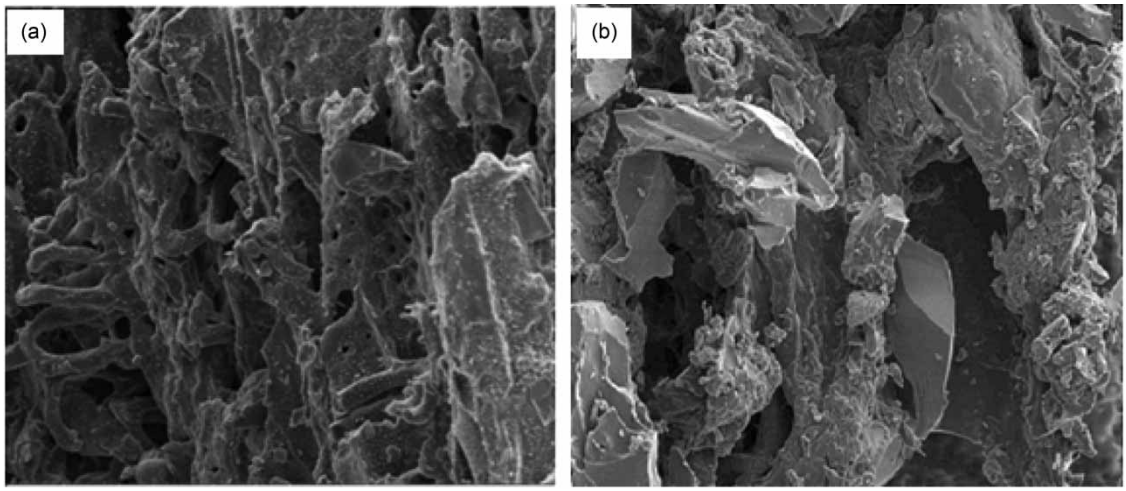

Figure 2 | SEM images of (a) BC and (b) BC-$MgCl_2$.

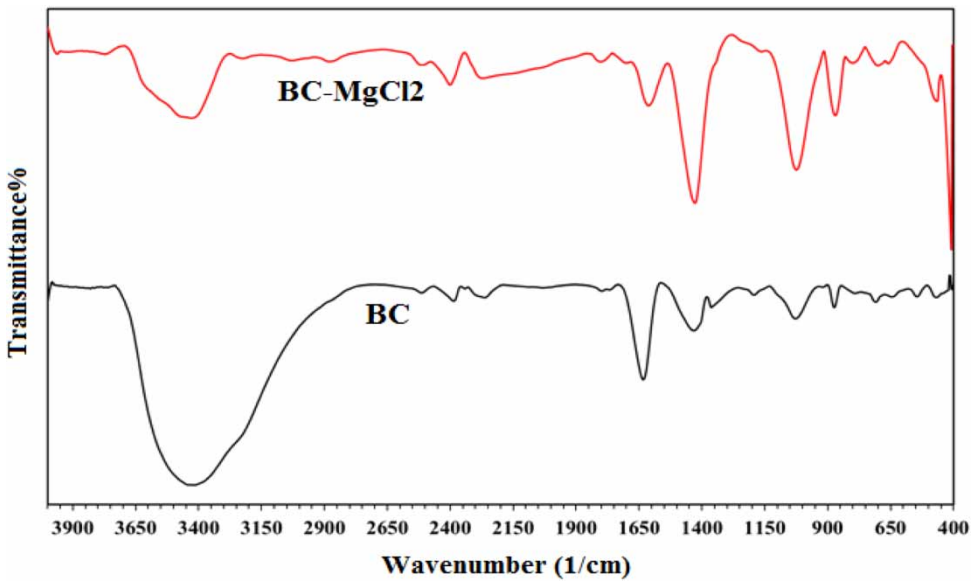

Figure 3 | FTIR spectra of BC and BC-$MgCl_2$.

band between 3,200 and 3,550 cm^{-1} shows the existence of OH groups and the vibration of N-H stretching. This band is stronger in BC than in the BC–$MgCl_2$, which could be attributed to the molecular interaction between $MgCl_2$ and activated carbon BC. The band located at about 2,300 cm^{-1} was ascribed to triple bonds such as nitriles and carbene groups. The bands located at 1,600 and 1,450 cm^{-1} correspond to olefinic C,C stretching and C-H in-plane bending vibrations in methyl and methylene groups. The intense band at 1,050 cm^{-1} belongs to C-O stretching vibrations in alcohols, phenols, and ether or ester groups. The band around 860 cm^{-1} may be attributed to the presence of carboxylic acid or alkyl halides.

Contact time and adsorbent dosage studies

It is well known that adsorption efficiency is heavily dependent on adsorption time. The effect of contact time in P, PMP and PNP adsorption was therefore observed. Figure 4 shows the effect of contact time on the adsorption of P, PMP and PNP by BC and BC-$MgCl_2$. As illustrated in Figure 4, P, PMP and PNP adsorption increased significantly up to the first 60 min, resulting in a total adsorption efficiency of q_e. A general observation was that the removal efficiency of P, PMP and PNP with increasing contact time, which is generally true for good adsorbents, is increasing before equilibrium (Liao *et al.* 2011). During the preliminary stage of adsorption, rapid adsorption was attributed to the availability of vacant surface sites and, after a certain period of time, the vacant sites are occupied by phenol molecules, which leads to a decrease in adsorption capacity due to a decrease in the adsorption sites available (Garba & Abdul 2016). The BC and BC-$MgCl_2$ q_e values for P, PMP and PNP removal are calculated as 22.989, 45.240, 58.310, 37.356, 98.253 and 117.126 mg/g, respectively.

It is well known that in a given initial concentration of adsorbent molecules in aqueous solution, adsorbent dose plays a very important role in determining the adsorption capacity. The effect of BC and BC-$MgCl_2$ dosages on the percentage removal (%Removal) of P, PMP and PNP was investigated for a range of adsorbent concentration (0.01–0.35 g) in 50 mL of 50 mg/L adsorbent concentration solution and findings are shown in Figure 5. The percentage of P, PMP and PNP removal increased with a rising adsorbent dose and reached a peak removal of approximately 74, 81, 88, 94, 89 and 98%, respectively, for BC and BC-$MgCl_2$. This may be due to an increase in the adsorbent surface area, increasing the number of adsorption sites available for adsorption. It can be seen that the peak percentage of removal of the BC and BC-$MgCl_2$ was usually highest at the beginning (0.20 g/50 mL), and thereafter no significant amount of these phenols was extracted from the solution, suggesting the saturation of the adsorption sites. These findings align well with what our recent previous research has stated (Mohammed *et al.* 2018; Hamadneh *et al.* 2019). Additional adsorption tests were performed with the 0.20 g/50 mL dose of BC and BC-$MgCl_2$ from the experimental results obtained.

Effects of pH and ionic strength

It is well known that solution pH influences both the adsorbent surface charge and the dissociation status of the phenolic species correlated with their constants of dissociation (pK_a). Phenols are ionizable and the degree of adsorption of phenolate anions to the geometric surface is primarily determined by the adsorbent's surface load,

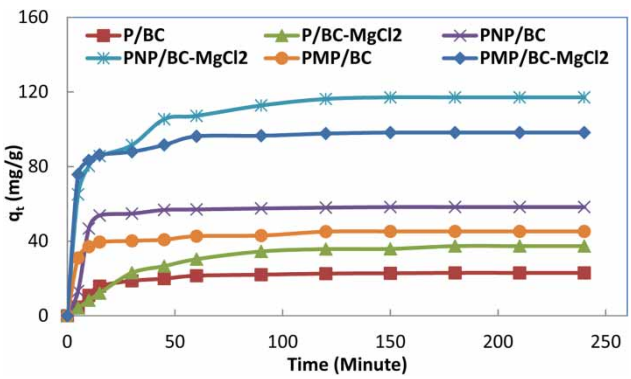

Figure 4 | The effect of contact time on the BC and BC-$MgCl_2$ adsorption capacities for P, PMP and PNP. Initial phenols concentration 50 mg/L; dosage of biochar 0.20 g/50 mL; pH = 7.0; time of contact 24 h; temperature 25 °C.

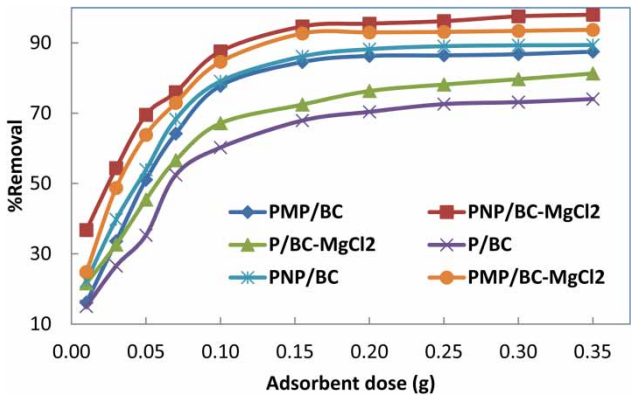

Figure 5 | The effect of adsorbent dosage on the BC and BC-$MgCl_2$ %Removal for P, PMP and PNP. Initial phenols concentration 50 mg/L; pH = 7.0; time of contact 24 h; temperature 25 °C.

Table 3 | Chemical structures and some properties of the P, PMP and PNP

Phenols	Structure	pK_a	Hydrophobic parameter	Water solubility (g/L)	Electron density on phenol ring
P	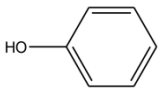	9.89	1.46	67	−0.508
PMP	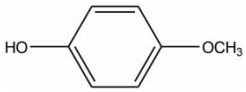	10.17	1.30	40	−0.397
PNP	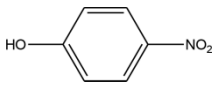	7.15	1.90	16	−0.086

which in turn is correlated with the pH_{pzc}. Therefore, it is necessary to determine the pH_{pzc} of the adsorbent to understand the adsorption process. It determines how quickly pollutants are adsorbed by an adsorbent. $PH > pH_{pzc}$ is favored for cationic adsorption and $pH < pH_{pzc}$ is recommended for anionic adsorption. The BC (9.71) and BC-$MgCl_2$ (6.92) pH_{pzc} were lower than the BC (10.22) and BC-$MgCl_2$ (8.69) pH suggesting abundance of negative charges on the surface of the activated carbon. The phenolic compounds examined in the present work have different values of pK_a, 9.89, 10.17 and 7.15, respectively, for P, PMP and PNP (Table 3).

To examine effect of pH on the adsorption of P, PMP and PNP, the batch equilibrium experiments were carried out at different pH values of 2–11, and results are as shown in Figure 6. The figure revealed that the q_e values of P, PMP and PNP were increasing slightly with increasing pH up to $pH = pK_a$ for each phenol and then decreased with further increasing pH when $pH > pK_a$. At lower pH, i.e., from pH 2 to pK_a values, the hydrophobic effects (Table 3), π–π^* interaction and hydrogen-bonding interaction played an essential role in the adsorption of P, PMP and PNP on the BC and BC-$MgCl_2$ surfaces. This could be because phenols exist as a neutral molecule at $pH < pK_a$, and the deprotonation process starts at around pK_a. The decreasing of BC and BC-$MgCl_2$ adsorption of P, PMP and PNP at higher pH could be explained on the assumption that the negative charge covering the activated carbon surfaces increased the electrochemical repulsion forces between phenol anionic form and the activated carbon surfaces. Similar results have been found by our previous work and other researchers (Soto *et al.* 2011; Parker *et al.* 2013; Mohammed *et al.* 2018; Houari *et al.* 2014).

The influence of ionic strength on the P, PMP and PNP adsorption on the BC and BC-$MgCl_2$ is shown in Figure 7. It can be seen that the increase in ionic strength from 0.01 to 0.20 M NaCl resulted in the slight decrease in the amount of P, PMP and PNP adsorbed onto the BC and BC-$MgCl_2$. The deceased adsorption capacity of BC and BC-$MgCl_2$ with an increase in the NaCl concentration is possibly attributed to electrostatic attraction between the negatively charged activated carbon surface and Na^+. These electrostatic attraction

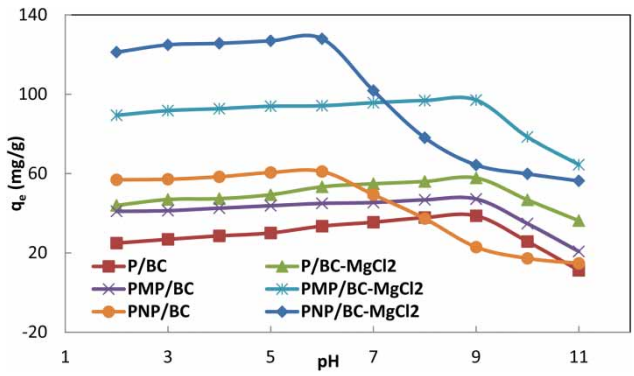

Figure 6 | The effect of pH on the BC and BC-$MgCl_2$ adsorption capacities for P, PMP and PNP. Initial phenols concentration 50 mg/L; dosage of biochar 0.20 g/50 mL; time of contact 24 h; temperature 25 °C.

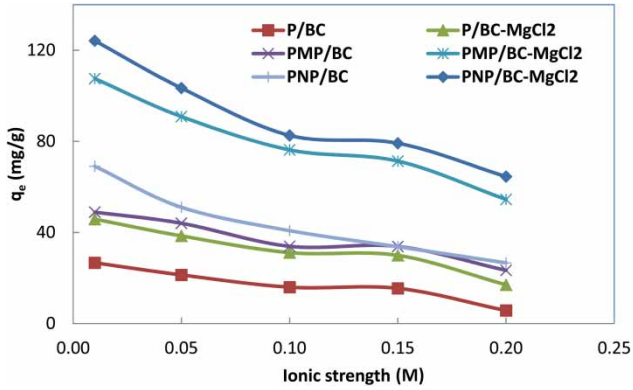

Figure 7 | The effect of ionic strength on the BC and BC-$MgCl_2$ adsorption capacities for P, PMP and PNP. Initial phenols concentration 50 mg/L; dosage of biochar 0.20 g/50 mL; pH = 7.0; time of contact 24 h; temperature 25 °C.

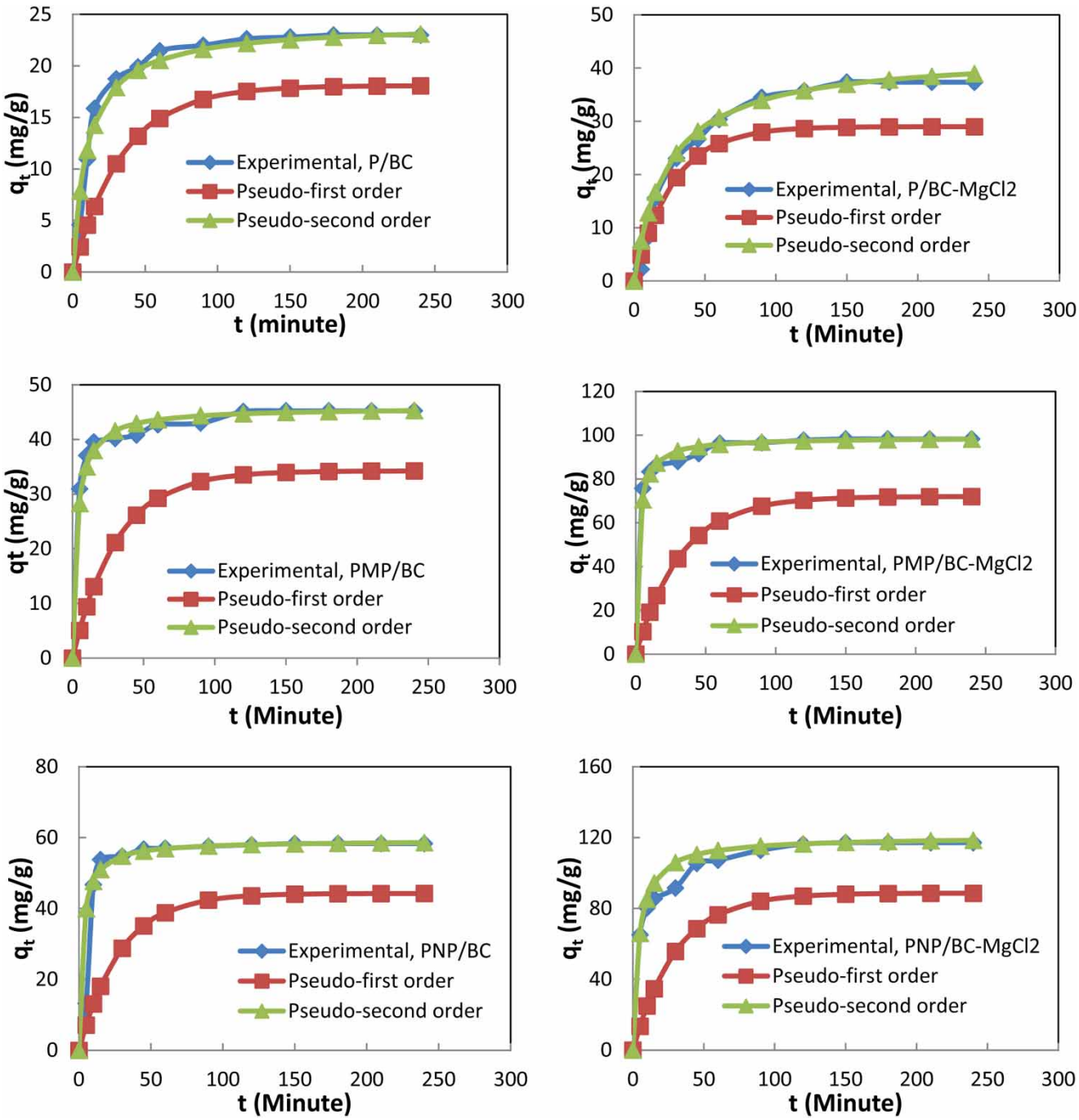

Figure 8 | Kinetic-model fits for adsorption of P, PMP and PNP on BC and BC-$MgCl_2$. Initial phenols concentration 50 mg/L; dosage of biochar 0.20 g/50 mL; pH = 7.0; time of contact 24 h; temperature 25 °C.

forces prevent activated carbon particles and phenols from being very close to each other; as a consequence, the adsorption capacity of the activated carbon for phenols will decrease. This outcome demonstrates the increasing competition between phenol molecules and Na^+ ions for available adsorbing sites on the activated carbon surface when the salt concentration increases.

Adsorption kinetics

Two kinetic models were used to study the adsorption kinetics of P, PMP and PNP on BC and BC-$MgCl_2$ experimental outcomes: Lagergren pseudo-first order (which was the most accurate and appropriate model for original quick reaction) and pseudo-second pseudo ist also

given in figs order (which was presumed to depend on the amount of active locations on the adsorbent surface as a rate control phase. The kinetic information acquired from the nonlinear regression assessment appropriate for BC and BC-$MgCl_2$ together with R^2, χ^2 and $F_{error\%}$ are provided in Figure 8 and listed in Table 4. The greater value of R^2 (>0.999), which was nearer to unity, and reduced χ^2 and $F_{error\%}$ values for P, PMP, and PNP adsorption on BC and BC-$MgCl_2$ (Table 4) for the pseudo-second order kinetic model show better information fitness, compared with the pseudo-first order model. It can also be seen that the adsorption capacity calculated by the dynamic model of the pseudo-second order ($q_{e.Calcd.}$) is much closer to the experiment values ($q_{e.Exp.}$). Thus, the above results indicate that the adsorption process follows the pseudo-second order kinetic model better than the pseudo-first order, suggesting that the P, PMP and PNP rates were proportional to the number of active sites on the BC and BC-$MgCl_2$ surfaces. For the adsorption of phenols on graphene oxide, Wang *et al.* (2014) recorded comparable observations.

Effect of phenolic molecular structure on adsorption isotherms

The adsorption data were analyzed using the two-parameter isotherm models of Langmuir, Freundlich, and D-R isotherm equations (Equations (6)–(9)). The three models were assessed by nonlinear regression analysis in the study. The adsorption equilibrium isotherms are shown in Figure 9, and the constant parameters and linear correlation coefficient (R^2), chi-squared (χ^2) and error function $F_{error\%}$ at 25, 35 and 45 °C are tabulated in Tables 5 and 6. From these results, it can be concluded that Langmuir and D-R models are more suitable for the adsorption process than Freundlich model by comparing the values of R^2, χ^2 and $F_{error\%}$.

The model of Langmuir adsorption is based on the assumption of homogeneous surface locations for monolayer adsorption. The D–R isotherm is more general than the Langmuir isotherm because it assumes no homogeneous surface or potential for continuous adsorption. The applicability of the isothermic models Langmuir and D-R to the six structures means that both monolayer adsorption and heterogeneous surface conditions exist. The monolayer adsorption capacities for P, PMP and PNP onto BC and BC-$MgCl_2$ at 25 °C were 24.938, 45.455, 61.728, 43.860, 98.039 and 121.951 mg/g, respectively.

The Freundlich constant n is a measure of the deviation from linearity of the adsorption. If a value for n is above unity, adsorption is favorable. In particular, the value of n obtained for the six systems is significantly higher than unity at all the temperatures studied (Tables 5 and 6). The mean adsorption free energy E_{DR} (kJ/mol) can be calculated from D-R isotherm constant K_{DR} (mol^2/kJ^2) using Equation (9), and provides information on the physical or chemical nature of the adsorption mechanism: E_{DR} within the range of 1–8 kJ/mol indicates that physical adsorption occurs; between 8 and 16 kJ/mol, ion exchange adsorption; and when E_{DR} is between 20 and 40 kJ/mol, chemisorption is

Table 4 | Pseudo-first-order and pseudo-second-order adsorption rate constant and calculated $q_{e.Calcd.}$ and experimental values for the adsorption of P, PMP and PNP on BC and BC-$MgCl_2$ at 25 °C

	Pseudo-first order					Pseudo-second order				
$q_{e,Exp.}$ (mg/g)	k_1 min^{-1}	$q_{e,Calcd.}$ (mg/g)	R^2	χ^2	$F_{error\%}$	k_2 (g/mg·min)	$q_{e,Calcd.}$ (mg/g)	R^2	χ^2	$F_{error\%}$
P/BC										
24.938	0.029	18.084	0.7769	15.52	34.75	0.004	24.096	0.9997	0.29	4.54
PMP/BC										
45.455	0.032	34.253	0.7880	17.18	32.31	0.007	45.872	0.9993	0.27	2.70
PNP/BC										
61.728	0.035	14.463	0.7453	14.42	31.41	0.007	59.172	0.9994	0.16	1.89
P/BC-$MgCl_2$										
43.860	0.037	28.991	0.9722	15.76	25.91	0.001	42.735	0.9999	0.31	3.56
PMP/BC-$MgCl_2$										
98.039	0.031	72.019	0.7981	28.61	23.32	0.005	99.010	0.9992	0.37	2.11
PNP/BC-$MgCl_2$										
121.951	0.033	58.616	0.6414	18.76	16.06	0.002	120.482	0.9995	1.31	4.96

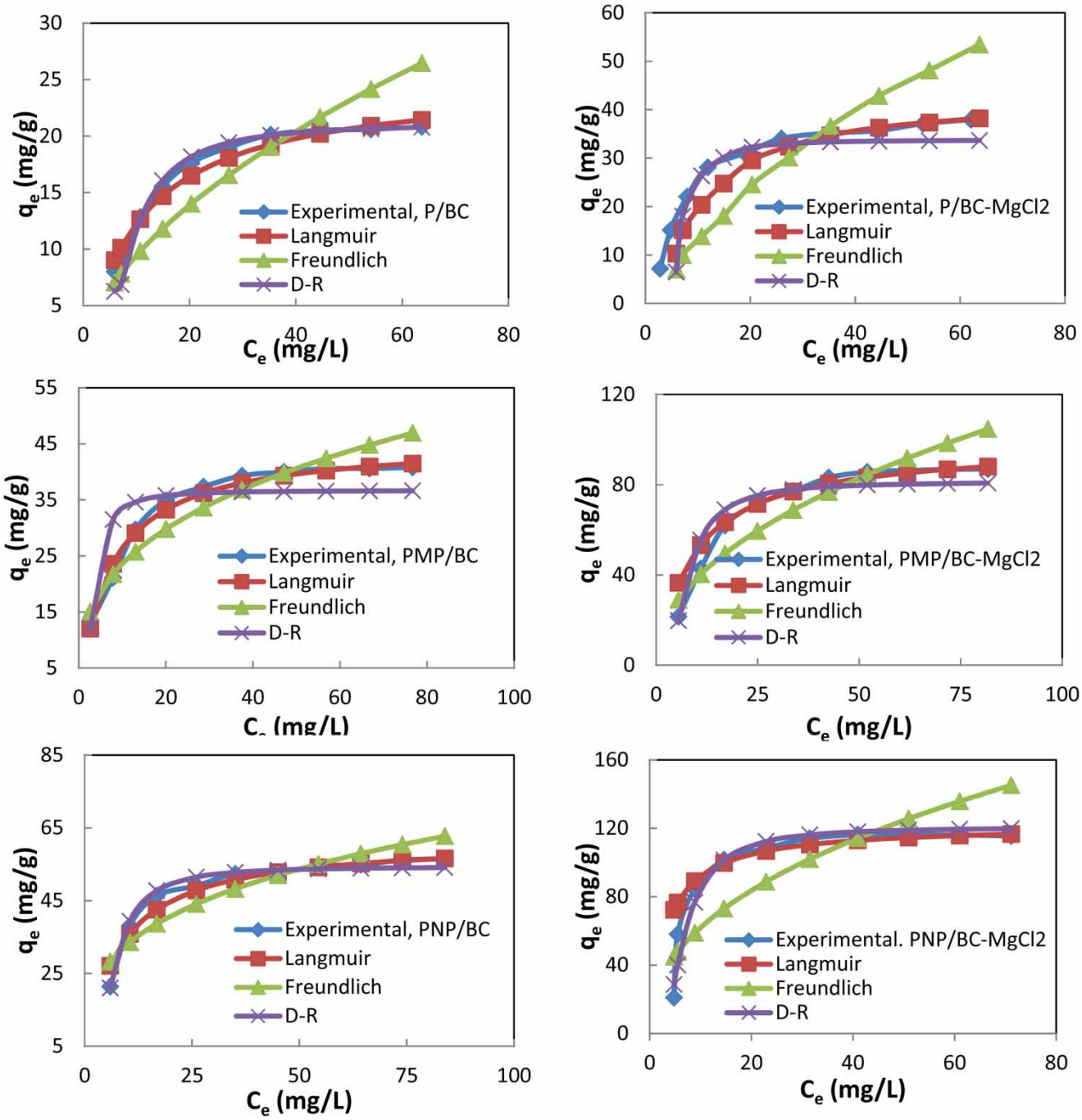

Figure 9 | Isotherm-model fits for adsorption of P, PMP and PNP on BC and BC-$MgCl_2$. Initial phenols concentration 10–100 mg/L; dosage of biochar 0.20 g/50 mL; pH = 7.0; time of contact 24 h; temperature 25 °C.

indicated (Dubinin *et al.* 1947). For the six systems, the E_{DR} calculated was 2.168 to 6.521 kJ/mol (Tables 5 and 6), indicating that P, PMP and PNP are likely to be removed primarily through physical adsorption.

To study the effect of molecular structure on adsorption, three phenolic compounds were considered (Table 3): P, which has no substituent on phenol; PMP, which has electron donating group on phenol; and PNP, which has electron withdrawing group on phenol. The BC and BC-$MgCl_2$ adsorption capacity increases in the order of $P <$ PMP < PNP. This trend can be interpreted by two factors: electron density on the phenol ring and the solubility of

Table 5 | Parameters of the Langmuir, Freundlich and D-R adsorption model for P, PMP and PNP onto BC at different temperatures

	P			PMP			PNP		
Parameters	**25 °C**	**35 °C**	**45 °C**	**25 °C**	**35 °C**	**45 °C**	**25 °C**	**35 °C**	**45 °C**
Langmuir									
q_{max} (mg/g)	24.938	20.080	15.291	45.455	39.841	37.175	61.728	56.180	46.512
K_L (L/mg)	0.002	0.005	0.006	0.001	0.002	0.004	0.007	0.019	0.036
R_L	0.094	0.123	0.053	0.069	0.038	0.101	0.070	0.074	0.044
R^2	0.9611	0.9641	0.9942	0.9967	0.9998	0.9954	0.9826	0.9999	0.9981
χ^2	0.56	0.46	0.42	0.52	0.51	0.48	1.18	1.16	1.08
$F_{error\%}$	7.24	6.87	6.28	4.89	4.73	4.66	6.06	5.99	5.74
Freundlich									
K_F [mg·g^{-1}(L·mg^{-1})1/n]	2.616	2.250	3.307	10.780	13.552	4.745	16.535	14.116	16.986
n	1.797	1.933	2.516	2.946	3.815	2.101	3.326	3.201	4.384
R^2	0.7824	0.8169	0.8003	0.8780	0.8639	0.8619	0.8431	0.7284	0.8792
χ^2	5.52	5.45	5.29	3.66	3.61	3.48	5.82	5.55	5.49
$F_{error\%}$	20.84	20.11	19.76	11.48	11.29	10.87	13.13	12.96	11.89
D-R									
q_{max} (mg/g)	21.115	15.037	12.748	36.690	35.416	29.961	54.407	46.201	42.356
E_{DR} (kJ/mol)	2.168	2.971	5.823	5.328	6.521	2.633	2.798	4.253	3.151
R^2	0.9757	0.9829	0.9767	0.9614	0.9314	0.9396	0.9785	0.8829	0.9244
χ^2	1.02	1.01	0.98	1.13	1.12	1.08	0.44	0.42	0.41
$F_{error\%}$	3.01	2.99	2.81	4.39	3.86	3.65	3.12	2.85	2.44

phenolic compounds in water (Table 3). The order of electron density on the phenol ring, P (−0.508) > PMP (−0.397) > PNP (−0.086) (Parker *et al.* 2013), demonstrates a close correlation to the above trend. In the case of PNP, by the addition of electron with drawing groups, there is less electron density on the phenol ring leading to better uptake, indicative of adsorption through π–π interactions between the BC and BC-$MgCl_2$ surface and the PNP (Dabrowski *et al.* 2005). Since the solubility of the phenolics is a measure of the adsorbed solvent forces of the attraction, any change in the solubility of a molecule can impact target forces that adsorb. If we consider the solubility of the phenolics used in the present work, the trend is PNP (16 g/L) < PMP (40 g/L) < P (67 g/L), which is in accordance with the literature (Wang *et al.* 2014) stating that a hydrophobic substance would be more likely to be adsorbed from aqueous solution.

Comparison of P, PMP and PNP adsorption on BC and BC-$MgCl_2$ with other data from the literature are presented in Table 7. Comparing the q_{max} values with those reported earlier for adsorption of P, PMP and PNP showed that the q_{max} values for phenolic compounds studied here are 1–2 orders larger than those of activated carbon studied previously. From these results it may be concluded that activated carbon derived from olive waste and modified with $MgCl_2$ is an effective adsorbent for removal of phenolic compounds from aqueous solution.

Adsorption thermodynamics

The thermodynamic parameters of a reaction, including the changes in Gibbs energy (ΔG^o), entropy (ΔS^o), and enthalpy (ΔH^o), can be considered as indicators for practical applications. These parameters can be computed according to the laws of thermodynamics using the following equations:

$$\Delta G^o = -RT \ln K_d \tag{15}$$

The K_d can be easily obtained as a dimensionless parameter by multiplying K_L by the molecular weight of adsorbate (P; 94, PMB; 124 and PNP; 139 g/mol), 1000, and then 55.5 (the number of moles of pure water per liter) (Tran *et al.* 2017a, 2017b; Lima *et al.* 2019; Lima *et al.* 2020).

Table 6 | Parameters of the Langmuir, Freundlich and D-R adsorption model for P, PMP and PNP onto BC-$MgCl_2$ at different temperature

	P			PMP			PNP		
Parameters	**25 °C**	**35 °C**	**45 °C**	**25 °C**	**35 °C**	**45 °C**	**25 °C**	**35 °C**	**45 °C**
Langmuir									
q_{max} (mg/g)	43.860	40.816	37.594	98.039	90.090	86.957	121.951	113.636	104.167
K_L (L/mg)	0.008	0.012	0.025	0.028	0.046	0.059	0.018	0.054	0.154
R_L	0.084	0.133	0.098	0.085	0.063	0.083	0.032	0.072	0.039
R^2	0.9681	0.9226	0.9693	0.9888	0.9992	0.9959	0.9701	0.9973	0.9972
χ^2	1.19	1.11	1.06	1.49	1.37	1.22	1.02	0.98	0.90
$F_{error\%}$	3.59	3.29	3.08	5.53	5.14	4.87	6.43	6.23	6.12
Freundlich									
K_F [mg·g^{-1}(L·mg^{-1})1/n]	3.563	4.140	6.611	12.877	25.351	15.406	22.809	29.054	33.791
n	1.168	1.847	2.479	2.101	3.432	2.508	2.306	3.205	3.674
R^2	0.7846	0.7545	0.7773	0.8591	0.8618	0.8471	0.8617	0.8757	0.7436
χ^2	13.45	12.83	12.08	13.96	12.99	12.37	15.88	14.73	14.69
$F_{error\%}$	16.01	15.97	15.26	16.64	16.33	16.12	29.94	29.58	29.14
D-R									
q_{max} (mg/g)	33.822	31.174	30.960	81.321	73.369	73.083	120.723	98.435	96.950
E_{DR} (kJ/mol)	4.157	2.527	2.643	2.462	6.090	2.728	2.784	2.864	4.011
R^2	0.9850	0.9928	0.9286	0.9717	0.8985	0.9370	0.9918	0.9451	0.9928
χ^2	1.59	1.43	1.39	1.92	1.85	1.81	1.39	1.31	1.28
$F_{error\%}$	6.75	6.63	6.18	7.37	7.24	6.84	7.85	7.29	7.14

The relationship between ΔG^o, ΔH^o and ΔS^o is described as:

$$\Delta G^o = \Delta H^o - T\Delta S^o \tag{16}$$

The well-known van't Hoff equation is obtained by substituting Equation (15) into Equation (16)

$$\ln K_d = -\frac{\Delta H^o}{RT} + \frac{\Delta S^o}{R} \tag{17}$$

where R and T represent the universal gas constant (8.314 J/mol·K) and the system temperature (K). ΔG^o can be directly calculated from Equation (15), while ΔH^o and ΔS^o were determined from the slope and intercept, respectively, of a plot of lnK_d against $1/T$ (Equation (17)) figure not shown). The thermodynamic parameters ΔG^o, ΔH^o and ΔS^o are listed in Table 8.

At each temperature, the adsorption of P, PMP and PNP on BC and BC-$MgCl_2$ had negative ΔG^o, showing that the adsorption phenomenon occurred favorably and spontaneously with minimal requirements of the adsorption energies. This result was in good agreement with the conclusions drawn from the Freundlich exponent n obtained from the isotherm study described in the above section.

A physisorption process usually yields ΔG^o values between −0 and −40 kJ/mol, while chemisorption yields ΔG^o values between −800 and −400 kJ/mol (Yousef *et al.* 2011). The values of ΔG^o in the present work ranged from −19.077 to −36.997 kJ/mol. The adsorption of P, PMP and PNP on BC and BC-$MgCl_2$ was therefore a process of physisorption.

When the temperature decreased from 45 to 25 °C, the magnitude of free energy transition (ΔG^o) moved to the higher negative value, indicating that the adsorption at low temperature is more spontaneous. Similar results have been published for the free energy of extracting phenolic compounds by several researchers (Khenniche & Benissad 2010; Salam & Burk 2010).

The positive value of ΔH^o indicates that BC and BC-$MgCl_2$ adsorption of P, PMP and PNP is an endothermic reaction consistent with temperature influence. Positive values of ΔS^o affirm the solution's dissociative mechanism and the increasing degree of phenolic freedom. Therefore,

Table 7 | Comparison of the maximum adsorption capacity (q_{max}) for the adsorption of P, PMP and PNP on various adsorbents

		Conditions			
Adsorbent	**Adsorbate**	**pH**	**T (°C)**	**q_{max} (mg/g)**	**Reference**
Bamboo biochar	P	–	25	126.734	Yang *et al.* (2016)
	PNP			172.981	
Activated wood coal	P	5.0	25	5.64	Houari *et al.* (2014)
	PNP			20.85	
Starbon of starch	P	11.0	25	87.21	Parker *et al.* (2013)
	PMP		25	118.60	
Coconut coir pith	P	9.0	30	37.0	Soto *et al.* (2011)
Graphene oxide	P	6.0	25	45.402	Wang *et al.* (2014)
	PMP			102.796	
	PNP			185.426	
Magnetic biochar	PNP	7.8	25	44.54	Ma *et al.* (2019)
Pine fruit shells	P	6.5	25	26.738	Mohammed *et al.* (2018)
Oil palm biochar	P	6.5	25	49.74	Lawal *et al.* (2020)
Organo-functional biochar	P	10	25	37.66	Mingliang *et al.* (2019)
BC	P	3.6	25	24.938	This work
	PMP			45.455	
	PNP			61.728	
BC-$MgCl_2$	P	5.5	25	43.860	This work
	PMP			98.039	
	PNP			121.951	

Table 8 | Thermodynamic parameters for the adsorption of P, PMP and PNP on BC and BC-$MgCl_2$

T	**ΔG^o kJ/mol**	**ΔH^o kJ/mol**	**ΔS^o kJ/K·mol**
	P/BC		
25 °C	−22.515	79.130	340.891
35 °C	−25.896		
45 °C	−29.334		
	PMP/BC		
25 °C	−19.077	104.041	414.719
35 °C	−24.897		
45 °C	−27.297		
	PNP/BC		
25 °C	−27.034	88.411	386.834
35 °C	−30.564		
45 °C	−34.786		
	P/BC-$MgCl_2$		
25 °C	−26.308	46.369	243.251
35 °C	−28.269		
45 °C	−31.194		
	PMP/BC-$MgCl_2$		
25 °C	−30.190	29.003	108.821
35 °C	−32.470		
45 °C	−34.154		
	PNP/BC-$MgCl_2$		
25 °C	−29.295	85.526	385.096
35 °C	−33.136		
45 °C	−36.997		

the arrangement of phenolics on the solid/solution interfaces becomes more random during the adsorption process.

CONCLUSIONS

In this study, adsorption of three phenolic compounds by low-cost activated carbon produced from olive oil solid waste (BC) and by BC chemically activated using $MgCl_2$ (BC-$MgCl_2$) using slow pyrolysis at 630 °C was characterized and investigated for efficient and effective removal of P, PMP and PNP. The study on adsorption mechanism indicated that P, PMP and PNP adsorption was mainly enhanced by introducing electron donating and withdrawing functional groups on the benzene ring. In the adsorption process, P, PMP and PNP adsorption on BC and BC-$MgCl_2$ was a spontaneous, endothermic reaction and entropy-increasing process which was more in line with pseudo-second order kinetic model and Langmuir and D-R isotherm models. The maximum adsorption capacity for P, PMP and PNP onto BC and BC-$MgCl_2$ was in the order of PNP > PMP > P.

REFERENCES

Abdel-Ghani, N. T., Rawash, E. S. A. & El-Chaghaby, G. A. 2016 Equilibrium and kinetic study for the adsorption of p-nitrophenol from wastewater using olive cake based activated carbon global. *Journal of Environmental Science and Management* **2** (1), 11–18.

Angın, D., Altintig, E. & Kose, T. E. 2013 Influence of process parameters on the surface and chemical properties of activated carbon obtained from biochar by chemical activation. *Bioresource Technology* **148**, 542–549.

Baccar, R., Sarrà, M., Bouzid, J., Feki, M. & Blanquez, P. 2012 Removal of pharmaceutical compounds by activated carbon

prepared from agricultural by-product. *Chemical Engineering Journal* **211–212**, 310–317.

Cardoso, C. R. & Ataide, C. H. 2015 Micropyrolysis of tobacco powder at 500 °C: influence of $ZnCl_2$ and $MgCl_2$ contents on the generation of products. *Chemical Engineering Communication* **202**, 484–492.

Cha, J. S., Park, S. H., Jung, S. C., Ryu, C., Jeon, J. K., Shin, M. C. & Park, N. Y. 2016 Production and utilization of biochar: a review. *Journal of Industrial and Engineering Chemistry* **40**, 1–15.

Cimino, G., Cappello, R. M., Caristi, C. & Toscano, G. 2005 Characterization of carbons from olive cake by sorption of wastewater pollutants. *Chemosphere* **61**, 947–955.

Dabrowski, A., Podkoscielny, P., Hubicki, Z. & Barczak, M. 2005 Adsorption of phenolic compounds by activated carbon–a critical review. *Chemosphere* **58**, 1049–1070.

Dubinin, M. M., Zaverina, E. D. & Radushkevich, L. V. 1947 Sorption and structure of active carbon. 1: Adsorption of organic vapors. *The Journal of Physical Chemistry A* **21**, 1351–1362.

El Hanandeh, A. 2013 Carbon abatement via treating the solid waste from the Australian olive industry in mobile pyrolysis units: LCA with uncertainty analysis. *Waste Management & Research* **31** (4), 341–352.

El Hanandeh, A., Abu-Zuryk, R. A., Hamadneh, I. & Al-Dujaili, A. H. 2016 Characterization of biochar prepared from slow pyrolysis of Jordanian olive oil processing solid waste and adsorption efficiency of Hg^{2+} ions in aqueous solutions. *Water Science and Technology* **74** (8), 1899–1910.

Freundlich, H. M. F. 1906 About the adsorption. *Zeitschrift für Physikalische Chemie* **57**, 385–470.

Garba, Z. N. & Abdul, A. 2016 Evaluation of optimal activated carbon from an agricultural waste for the removal of para-chlorophenol and 2,4-dichlorophenol. *Process Safety and Environmental Protection* **102**, 54–63.

Gaya, U. I., Otene, E. & Abdullah, A. H. 2015 Adsorption of aqueous Cd(II) and Pb(II) on activated carbon nanopores prepared by chemical activation of doum palm shell. *SpringerPlus* **4**, 458–476.

Hall, K. E., Calderon, M. J., Spokas, K. A., Cox, L., Koskinen, W. C., Novak, J. & Cantrell, K. 2014 Phenolic acid sorption to biochars from mixtures of feedstock materials. *Water Air & Soil Pollution* **225** (7), 1–9.

Hamadneh, I., Alatawi, A., Zalloum, R., Albuqain, R., Alsotari, S., Khalili, F. I. & Al-Dujaili, A. H. 2019 Comparison of Jordanian and standard diatomaceous earth as an adsorbent for removal of Sm(III) and Nd(III) from aqueous solution. *Environmental Science and Pollution Research* **26**, 20969–20980.

Han, Y., Boateng, A. A., Qi, P. X., Lima, I. M. & Chang, J. 2013 Heavy metal and phenol adsorptive properties of biochars from pyrolyzed switchgrass and woody biomass in correlation with surface properties. *Journal of Environmental Management* **118**, 196–204.

Houari, M., Hamdi, B., Bouras, O., Bollinger, J. C. & Baudu, M. 2014 Static sorption of phenol and 4-nitrophenol onto composite geomaterials based on montmorillonite, activated carbon and cement. *Chemical Engineering Journal* **255**, 506–512.

Hubbe, M. A., Azizian, S. & Douven, S. 2019 Implications of apparent pseudo-second-order adsorption kinetics onto cellulosic materials. A review. *BioResources* **14** (3), 7582–7626.

International Olive Council 2015 *World Olive Oil Figures*. International Olive Council, Madrid, Spain.

Khenniche, L. & Benissad, A. F. 2010 Adsorptive removal of phenol by coffee residue activated carbon and commercial activated carbon: equilirium, kinetics and thermodynamics. *Journal of Chemical Engineering* **55**, 4677–4686.

Lagergren, S. 1898 About the theory of so-called adsorption of soluble substances. *Kungliga Svenska Vetenskapsakademiens Handlingar* **24**, 1–39.

Langmuir, I. 1918 The adsorption of gases on plane surface of glass, mica and platinum. *Journal of the American Chemical Society* **40**, 1361–1403.

Lawal, A. A., Hassan, M. A., Ahmad Farid, M. A., Yasim-Anuar, T. A. T., Mohd Yusoff, M. Z., Zakaria, M. R., Roslan, A. M., Mokhtar, M. N. & Shirai, Y. 2020 One-step steam pyrolysis for the production of mesoporous biochar from oil palm frond to effectively remove phenol in facultatively treated palm oil mill effluent. *Environmental Technology & Innovation*, doi: https://doi.org/10.1016/ j.eti.2020.100730.

Lehmann, J., Rillig, M. C., Thies, J., Masiello, C. A., Hockaday, W. C. & Crowley, D. 2011 Biochar effects on soil biota–a review. *Soil Biology and Biochemistry* **43** (9), 1812–1836.

Li, H., Mahyoub, S. A. A., Liao, W., Xia, S., Zhao, H., Guo, M. & Ma, P. 2017 Effect of pyrolysis temperature on characteristics and aromatic contaminants adsorption behavior of magnetic biochar derived from pyrolysis oil distillation residue. *Bioresource Technology* **223**, 20–26.

Liao, S. W., Lin, C. I. & Wang, L. H. 2011 Kinetic study on lead(II) ion removal by adsorption onto peanut hull ash. *Journal of the Taiwan Institute of Chemical Engineers* **42**, 166–172.

Lima, E. C., Bandegharaei, A.-H., Piraján, J. C.-M. & Anastopoulos, I. 2019 A critical review of the estimation of the thermodynamic parameters on adsorption equilibria. Wrong use of equilibrium constant in the Van't Hoof equation for calculation of thermodynamic parameters of adsorption. *Journal of Molecular Liquids* **273**, 425–434.

Lima, E. C., Gomes, A. A. & Tran, H. N. 2020 Comparison of the nonlinear and linear forms of the van't Hoff equation for calculation of adsorption thermodynamic parameters (ΔS° and ΔH°). *Journal of Molecular Liquids*, https://doi.org/ 10.1016/ j.molliq.2020.113315).

Ma, F.-F., Zhao, B.-W., Diao, J.-R. & Jiang, Y.-F. 2019 Adsorption characteristics of p-nitrophenol removal by magnetic biochar. *China Environmental Science* **39** (1), 170–178.

Mall, I. D., Srivastava, V. C., Kumar, G. V. A. & Mishra, I. M. 2006 Characterization and utilization of mesoporous fertilizer plant waste carbon for adsorptive removal of dyes from aqueous solution. *Colloids and Surfaces A* **278**, 175–187.

Michailof, C., Stavropoulos, G. G. & Panayiotou, C. 2008 Enhanced adsorption of phenolic compounds, commonly

encountered in olive mill wastewaters, on olive husk derived activated carbons. *Bioresource Technology* **99**, 6400–6408.

Mingliang, G., Xubin, W., Mingyi, D., Guodong, L., Guoqing, H. & Jahangir, A. S. M. 2019 Adsorption analyses of phenol from aqueous solutions using magadiite modified with organo-functional groups: kinetic and equilibrium studies. *Materials* **12**, 1–16.

Mohammed, N. A. S., Abu-Zurayk, R. A., Hamadneh, I. & Al-Dujaili, A. H. 2018 Phenol adsorption on biochar prepared from the pine fruit shells: equilibrium, kinetic and thermodynamics studies. *Journal of Environmental Management* **226**, 377–385.

Mohan, D., Sarswat, A., Ok, Y. S. & Pittman, C. U. 2014 Organic and inorganic contaminants removal from water with biochar, a renewable, low cost and sustainable adsorbent – a critical review. *Bioresource Technology* **160**, 191–202.

Parker, H. L., Budarin, V. L., Clark, J. H. & Hunt, A. J. 2013 Use of starbon for the adsorption and desorption of phenols. *ACS Sustainable Chemistry and Engineering* **1**, 1311–1318.

Salam, M. A. & Burk, R. C. 2010 Thermodynamics and kinetics studies of pentachlorophenol adsorption from aqueous solutions by multiwalled carbon nanotubes. *Water Air and Soil Pollution* **210**, 101–111.

Soto, M. L., Moure, A., Domínguez, H. & Parajo, J. C. 2011 Recovery, concentration and purification of phenolic compounds by adsorption: a review. *Journal of Food Engineering* **105**, 1–27.

Sy, O. & Yd, S. 2016 Sorption of halogenated phenols and pharmaceuticals to biochar: affecting factors and mechanisms. *Environmental Science and Pollution Research* **23** (2), 951–961.

Tan, X., Liu, Y., Zeng, G., Wang, X., Hu, X., Gu, Y. & Yang, Z. 2015 Application of biochar for the removal of pollutants from aqueous solutions. *Chemosphere* **125**, 70–85.

Tazibet, S., Velasco, L. F., Lodewyckx, P., Abou M'Hamed, D. & Boucheffa, Y. 2018 Study of the carbonization temperature for a chemically activated carbon: influence on the textural and structural characteristics and surface functionalities. *Journal of Porous Materials* **25** (2), 329–340.

Toumi, K. H., Benguerba, Y., Erto, A., Dotto, G. L., Khalfaoui, M., Tiar, C., Nacef, S. & Amrane, A. 2018a Molecular modeling of cationic dyes adsorption on agricultural Algerian olive cake waste. *Journal of Molecular Liquids* **264**, 127–133.

Toumi, K. H., Bergaoui, M., Khalfaoui, M., Benguerba, Y., Erto, A., Dotto, G. L., Amrane, A., Nacef, S. & Ernst, B. 2018b Computational study of acid blue 80 dye adsorption on low cost agricultural Algerian olive cake waste: statistical mechanics and molecular dynamic simulations. *Journal of Molecular Liquids* **271**, 40–50.

Tran, H. N., You, S. J., Tran, H. N., You, S. J., Bandegharaei, A. H. & Chao, H. P. 2017a Mistakes and inconsistencies regarding adsorption of contaminants from aqueous solutions: a critical review. *Water Research* **120**, 88–116.

Tran, H. N., You, S. J. & Chao, H. P. 2017b Fast and efficient adsorption of methylene green 5 on activated carbon prepared from new chemical activation method. *Journal of Environmental Management* **188**, 1–14.

Ucar, S., Erdem, M., Tay, T. & Karagoz, S. 2009 Preparation and characterization of activated carbon produced from pomegranate seeds by $ZnCl_2$ activation. *Applied Surface Science* **255**, 8890–8896.

Vaghetti, J. C. P., Lima, E. C., Royer, B., Cardoso, N. F., Martins, B. & Calvete, T. 2009 Pecan nutshell as biosorbent to remove toxic metals from aqueous solution. *Separation Science and Technology* **44**, 615–644.

Vunain, E., Houndedjihou, D., Monjerezi, M., Muleja, A. A. & Kodom, B. T. 2018 Adsorption, kinetics and equilibrium studies on removal of catechol and resorcinol from aqueous solution using low-cost activated carbon prepared from sunflower (*Helianthus annuus*) seed hull residues. *Water Air and Soil Pollution* **229** (11), 366–389.

Wang, X., Huang, S., Zhu, L., Tian, X., Li, S. & Tang, H. 2014 Correlation between the adsorption ability and reduction degree of graphene oxide and tuning of adsorption of phenolic compounds. *Carbon* **69**, 101–112.

Weidemann, E., Niinipuu, M., Fick, J. & Jansson, S. 2018 Using carbonized low-cost materials for removal of chemicals of environmental concern from water. *Environmental Science and Pollution Research* **25** (16), 15793–15801.

Yang, T. & Lua, A. C. 2006 Textural and chemical properties of zinc chloride activated carbons prepared from pistachio-nut shells. *Materials Chemistry and Physics* **100**, 438–444.

Yang, K., Yang, J., Jiang, Y., Wu, W. & Lin, D. 2016 Correlations and adsorption mechanisms of aromatic compounds on a high heat temperature treated bamboo biochar. *Environmental Pollution* **210**, 57–64.

Yousef, R. I., El-Eswed, B. & Al-Muhtaseb, A. H. 2011 Adsorption characteristics of natural zeolites as solid adsorbents for phenol removal from aqueous solutions: kinetics, mechanism, and thermodynamics studies. *Chemical Engineering Journal* **171**, 1143–1149.

Zhang, P., Chang, C. C., Wang, R. & Zhang, S. 2014 Agricultural waste. *Water Environment Research* **86** (10), 1387–1415.

First received 25 December 2019; accepted in revised form 4 June 2020. Available online 18 June 2020